

Self-Sensing Morphing Wing using Shape Memory Alloy Actuator

Nuramirah Azid, Ermira Junita Abdullah *, Mohammad Yazdi Harmin

Department of Aerospace Engineering, Faculty of Engineering, Universiti Putra Malaysia, Serdang 43400, Selangor, Malaysia.

ABSTRACT

The aerodynamic efficiency of wing can be improved by using morphing wing system actuated by smart material. Shape memory alloy (SMA) can be used in such system to replace conventional actuator in order to reduce the weight of the wing. SMA acts as an actuator, embedded inside the wing to achieve the desired camber profile during flight. This study explores the self-sensing capability of the SMA by changing the resistivity during actuation using voltage drop across the SMA as the input to the feedback system. The self-sensing system can reduce the weight and cost as sensors can be eliminated. The SMA actuator was controlled using Proportional-Integral-Derivative (PID) controller with LabVIEW software where the voltage drop across the SMA acts as input to control the shape of the wing. The calibration data was critical to design the morphing wing actuation for the wind tunnel testing. The data was also analyzed to determine the voltage required to change the geometry of the morphing wing and improve the aerodynamics behavior in terms of lift-to-drag (L/D) ratio. The wing model was tested at angle of attack between -12° and 16° at wind speed of 20m/s. The experimental results of wind tunnel testing showed that the morphing wing system produced improvement on lift, drag and lift-to-drag ratio as predicted from earlier work using computational fluid dynamics. L/D improved as much as 9.2 at 4° AOA for SMA actuation of 3.5V and 10.79 at 6° AOA for SMA actuation of 4.8V.

Keywords: Morphing wing, Shape memory alloy, Feedback control, Self-sensing

I. INTRODUCTION

Each morphing technique for an aircraft is executed for different purpose but aims to either produce better aerodynamic performance or flight maneuverability. The change in airfoil shape affects the aerodynamics performance of the wing [1]. Morphing can either be globally on the whole wing or on specific part such as leading edge, trailing edge, camber or winglet [2-6]. Most of the morphing wing design uses conventional actuator but the mechanism can be improved by using smart material. By using smart actuator such as shape memory alloy (SMA), the entire wing can act as a unique control surface. SMA can be embedded into the morphing wing

and thus change the geometry shape by controlling its actuation. It has several advantages over conventional hydraulics including lighter weight, corrosion resistance and low power consumption [7]. SMA has unique thermomechanical properties as well as superelasticity behaviour that has been widely studied [8,9]. It has been classified as adaptive material being able to transform thermal energy into mechanical work as well as possess great damping capacity.

Smart material such as SMA has many advantages in producing wing with low maintenance cost and reduced complexity. SMA in the form of wire or spring can reduce the weight of the system as it is lightweight and compact, thus reducing the entire space inside the wing. For the

airfoil adjustment, it is mainly concerned with thickness variation. Airfoil adjustment can be achieved through camber change and this can be done by installing SMA at upper and lower part of the camber. Camber control provides an efficient means to improve L/D ratio at each flight condition. This concept is very convenient yet very simple compared to conventional motor that has greater complexity.

However, due to SMA's non-linearity and hysteresis behavior, a control feedback system is required to produce accurate actuation. There are many types of feedback system that has been developed using different input variables such as position, temperature, force and strain [10-12]. However, this increases the weight of the wing and the system's complexity. In order to improve the morphing wing system, other technique can be considered to simplify the system and reduce the required components. There is a potential to use the change in resistivity of the SMA during actuation as the input to the feedback system. From the literature, it shows there is great potential in self-sensing technique for accurate SMA actuation [13-18]. By using this technique, the system complexity is reduced further by eliminating sensor from the feedback system and instead utilizing the change of the behavior of the SMA actuator. In other words, it promotes the self-sensing capability of the SMA.

The research presented here considers the morphing wing system for aerospace application. Using self-sensing actuation will translate to even bigger savings in terms of cost, space and weight. Thus, the main objective of this study is to analyze the feasibility of self-sensing actuation for morphing wing application instead of using conventional actuator and external sensors. An experimental test bed of the morphing wing system was designed and the performance was analyzed under wind loading through wind tunnel experiment.

This paper presents the background on shape memory alloy as actuator used for morphing wing system, the methodology employed for the research, the experimental results i.e. the performance of the self-sensing shape memory alloy actuator control system and the performance of the morphing wing from the wind tunnel testing, the analysis of the results and main conclusion from the research conducted.

II. SHAPE MEMORY ALLOY ACTUATOR FOR MORPHING WING

Past history shows that morphing concept comes at a high cost, complex and also increases system's weight. This is due to the additional actuation system that could lead to weight penalty which will decrease the aerodynamic performance. However smart materials can overcome these limitations and enhance it by providing optimum design solution [19].

An actuator is a type of transducer or device that uses energy that comes from an electric current, hydraulic or pneumatic pressure and convert it into another form of energy. For example, motor convert energy from electricity into energy of a circular motion. While for linear actuator such as piezoelectric devices, the energy

comes from rotary motion and it will be converted into linear motion of energy. Actuators act as key elements of our aircrafts and the concept of electric aircraft forcing the development to substitute the use of hydraulics to electrical actuation [20].

Variable camber is a feature of aircraft wings to morph by changing the curvature of airfoil during flight. The control surfaces that help in cambering is ideally suited for aircraft application where it can be used throughout the flight regimes. For example, reshaping flaps and ailerons can be used in combination to provide camber control during cruising.

From a study conducted on variable geometry by the National Aeronautics and Space Administration (NASA), adjusting of camber resulted in increasing camber and deflection of trailing edge will improve the aerodynamics to the wing profile [21]. One technique is to adjust the curvature of camber line is chord-wise morphing [22].

For aerodynamics, camber represents the shape of the airfoil. If the camber is adjusted by means of actuation, this is known as camber control. Many methods can be applied to change the shape of the wing either at trailing edge, leading edge or even the whole part of the airfoil. This method is efficient as it can change the lift-to-drag (L/D) ratio depending on the flight condition and mission. To sum up, variable thickness of airfoil also can improve the aerodynamic performance similar to variable camber profile by chord wise morphing [23]

In a study, flexible skin is installed on the upper surface of the variable camber airfoil actuated by SMA [24]. Gas spring is vital when the SMA is inactive to counteract the pulling effect of aerodynamic forces over the flexible skin to un-morphed reference airfoil position. When the SMA is energized by the power supply, the pulling action causing load mode which the airfoil is in optimized morphing airfoil position. The actuation distance for each SMA is corresponding with the airfoil shape, and mechanical system of the SMA pulling the sliding rod and the action of gas spring. SMA will convert the horizontal movement along the span into the vertical motion perpendicular to the chord [24].

Shape memory alloy actuator has been demonstrated as a highly suitable option for morphing wing design with research spanning more than two decades. Currently, the focus is exploring new applications and techniques of morphing and also the improvement of system design [25-27].

Recent development in smart materials may overcome the weight, complexity and cost limitations of morphing wing. However, the design and integration of smart material embedded inside the morphing aircraft is challenging. To determine the best placement of the SMA wire actuators within the wing, many optimization methods that includes thermal, structural and aerodynamic analysis need to be utilized. Computational Fluid Dynamic (CFD) test has been conducted for hybrid Kevlar of NACA 0012 with shape memory alloy (SMA) as an actuator [23]. The selected position for the SMA is based on Finite Element Analysis (FEA) with high trailing edge deflection [28]. Analysis was done to show improvement of adaptive wing to the aerodynamic performance of the wing at sea

level environment by using GAMBIT and FLUENT with free stream velocity of 20m/s at different angle of attack. It was observed that lift coefficient is improved when shape of airfoil is cambered compared to symmetrical NACA 0012 airfoil. Lift curve shows a steady increase even though the airfoil is in zero degree of angle of attack. For the drag, the cambered produce lower drag for all angle of attack. This CFD result shows that camber airfoil can minimize the drag produce by the wing and increases the lift-to-drag ratio.

SMA has a distinctive combination of various novel properties including the shape memory effect, high damping capacity, good fatigue and wear resistance, high kinetic output per volume and, of significant importance, an excellent compatibility in various actuation system design [29]. The behavior of SMA is unique as it is non-linear in terms of thermal and mechanical properties. The changing shape can effectively increase the efficiency of a wing. SMA wire can be heated by power supply and cooled by reducing the current that flow across SMA. This simple actuation mechanism is widely used as linear actuators. In addition, SMAs are activated by changes in temperature. The non-linear behavior of SMA is because it exhibits unique crystalline characteristics which depends on applied stress and temperature but if controlled properly, it can act linearly over a range of temperature.

Another behaviour of SMA is the wires electrical resistance varies intrinsically when the material undergoes a phase changing from martensite to austenite and vice versa thus can be used as a sensing element in controlling actuator system. When heated, SMA wires will contract and change from martensite crystalline phase to austenite and vice versa when cooled. The Shape Memory Effect is one of the behaviour that attracts researchers to exploit this extraordinary behaviour to make linear actuator using SMA [30].

2.1 Feedback System for Shape Memory Alloy Actuator

SMA has non-linear response to the strain. Thus, linear control technique is not suitable for non-linear behavior SMA [28]. Previous study at E'cole de Technologie Supérieure, Canada substitute the SMA with linear rotary actuators and proved it is much easier integration in morphing wing CRIAQ 7.1 control actuation system. Thus, the challenge is to produce accurate control with response of strain input with compensation technique involving proportional and derivative control [30].

Smart composite can be controlled with SMA actuator using strain feedback system to control the deflection [11]. In this study, a temperature feedback system was also used and compared to the strain feedback system. Results show that strain feedback gives better performance with low overshoot, and no steady state error. Additionally, the power consumption is 40% less than the temperature feedback system.

Latest study shows that temperature feedback produces exceptional tracking performance. Large signal model based on temperature controller and small signal NPID controller with PWM gives this position of SMA wire at various loads. The control law and models used are

simple, easy to implement and run in real time. The temperature feedback controller is able to recover the disturbance and hysteresis of SMA [31].

Another study of temperature feedback is using hot water to actuate the SMA spring which then give impact on the morphology structure. As the temperature reaches 70-80°C, SMA spring will be compressed for the first few cycles followed by displacement loss in actuation. During this heating process, the length of the spring reduces and the mass moves upward proving the martensite to austenite changing phase. While when it cooled, the austenite changes to martensite phase and the length of the spring increases thus moves the mass downward. The application is suitable where there are no electrical connections, and in engines where it can replace the thermostat valves [32].

2.2 Resistivity Feedback of SMA

The electrical resistance through SMA is assumed to be constant at both phases of martensite and austenite. But one aspect that can change the resistivity of SMA is by applying constant load levels. The stress caused the resistivity to change linearly instead of being constant. There are 3 findings which allows the resistance behavior to be characterized in range of temperature, and stress [33]. These findings can be summarized as follows:

1. The resistance of SMA increases linearly with temperature both in martensite and austenite phase. The relation between temperature and resistivity of SMA is related with positive coefficient.
2. As the wire is heated, the resistivity is increase linearly and at certain point it drops to minimum and finally increase linearly again if there is further heating.
3. Peaks of maximum resistivity achieved as the increasing of wire stress cause the changes of temperatures in austenite and martensite phase and also absolute resistivity values in martensite phase.

Resistance plays a significant role in SMA self-sensing utilization while there has been little research that explains it due to the complexity of the SMA electrical resistivity. This resistivity is dependent on stress and temperature, but also the volume fractions of martensite, austenite and R-phase during the process which led to transformation [34].

The resistance changes linearly in martensite and austenite phases. Rate of change is larger in martensite phase compared with austenite phase. Electrical resistivity depends on stress, temperature, stress with or without temperature induced phase, R-phase distortion and martensite reorientation. SMA resistivity changes linearly with temperature and stress as with common metals behavior.

Wang et al [35] produced self-sensing model which shows data on SMA strain to resistance. The strain and resistance curves is repeatable throughout all the cycles and is stable even though there is the hysteresis gap between the cooling and heating process. The pattern for cooling and heating is the same in reverse direction separated with the hysteresis gap. Abdullah et al developed an experimental test bench for self-sensing displacement control in the range of 2mm using shape memory alloy

actuator [36]. It was found that the self-sensing feedback system was able to control the displacement and its accuracy was improved with pre-loading of the SMA actuator.

III. METHODOLOGY

3.1 Morphing Wing Design and Fabrication

An experimental test bed for the self-sensing morphing wing using shape memory alloy actuator was developed as a proof of concept to analyze the performance of the self-sensing SMA actuation system under wing loading. The morphing wing in this study was developed using the aerodynamics data that has been established on morphing wing with NACA 0012 airfoil [28]. The first step in designing the experimental test bed is to design the wing based on the aerodynamics data and to determine the size of the prototype for the given specifications of the wind tunnel. This included the SMA position inside the airfoil and current hook placement for the six component balance design. The next procedure was the actuator selection based on the NACA 0012 sizing. The

number of SMA wires was determined by the amount of force required to morph the wing and the SMA length was selected based on the amount of stroke required.

From the earlier FEM simulation, it has been determined that 6 wires are required to produce the force to morph the wing. Thus SMA characterization was done for 1 wire as a reference and 6 wires in order to determine the behaviour of the SMA during actuation. The morphing pattern of the airfoil was produced by the actuation of the SMA inside the wing controlled by the controller using LabVIEW software and compact DAQ hardware, and a proof of concept was conducted using wind tunnel testing. PID controller was designed for 1 and 6 SMA wires configuration.

The selection of the NACA 0012 airfoil was based on the previous study on the design and fabrication of hybrid composite adaptive wing structure [23]. This study includes the actuator placement of the SMA, according to analysis of Finite Element Analysis (FEA) and Computational Fluid Analysis (CFD). This airfoil parameter was build using Rhinoceros computer aided drawing software. The parameters are shown in Figure 2.

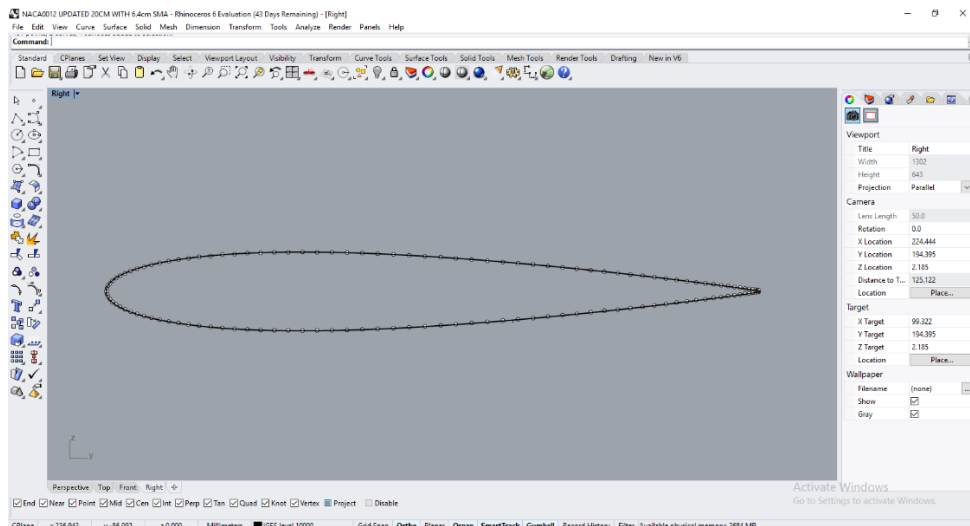


Figure 2 2D parameters of the NACA 0012

From Figure 3, it shows that the position of SMA at force node 3 and fixed node of 37. From leading edge, the SMA placement is at 9.1% for upper part, and 36.36% chord length for bottom part. These nodes were selected as the result shows that it will produce good camber profile

and maximum cambered with 6.51mm deflection of trailing edge. Figure 4 shows the 2D drawing of NACA 0012 with placement of SMA. Further detail drawing can be seen in Figure 5.

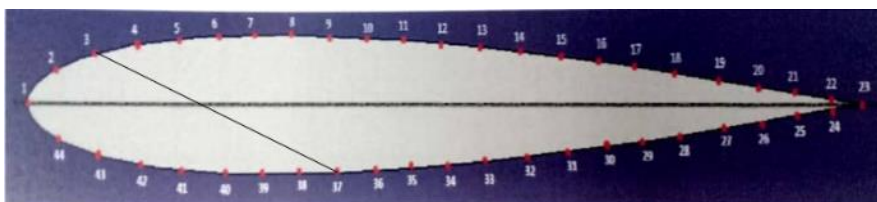


Figure 3 Position of SMA actuator

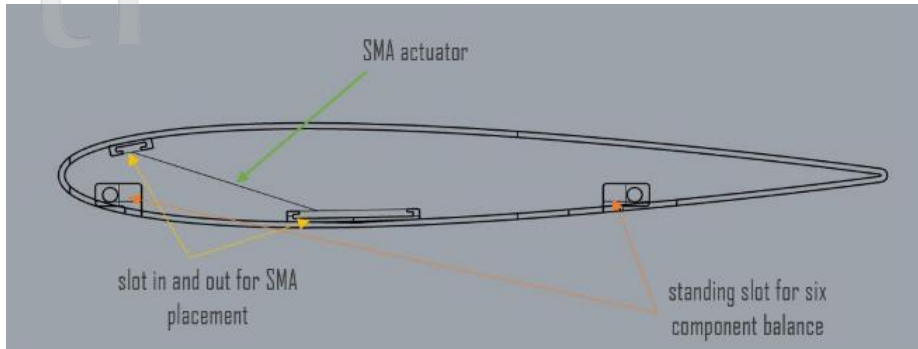


Figure 4 2D drawing of the SMA position inside the wing

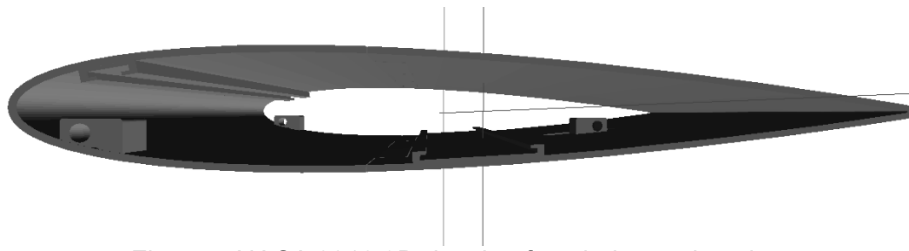


Figure 5 NACA 0012 3D drawing for wind tunnel testing

ABS with filament diameter 1.75mm was chosen for 3D printing along with the Zortrax M200 3D printer as it has excellent ductility, moderate strength and lightweight which was suitable for the morphing wing design as it can return to its original position in a short time after turning off the actuator. Additionally, it was easy to fabricate and low cost compared to other materials. The specification for this ABS is as shown in Table 1.

Figure 6 shows the wing model where it exceeded the planform area. Thus, the solution was to separate the wing model into 3 parts and print them separately as shown in Figures 7-9. A temporary standing was built along with the

airfoil part to ease the fabrication and avoid dimension error as shown in Figure 9. It was removed during the integration of the wing model.

Table 1 Mechanical properties of ABS

Property	Value
Young's Modulus (MPa)	2100
Poisson's ratio	0.392
Density (g/cm^3)	0.93673
Yield strength (MPa)	41

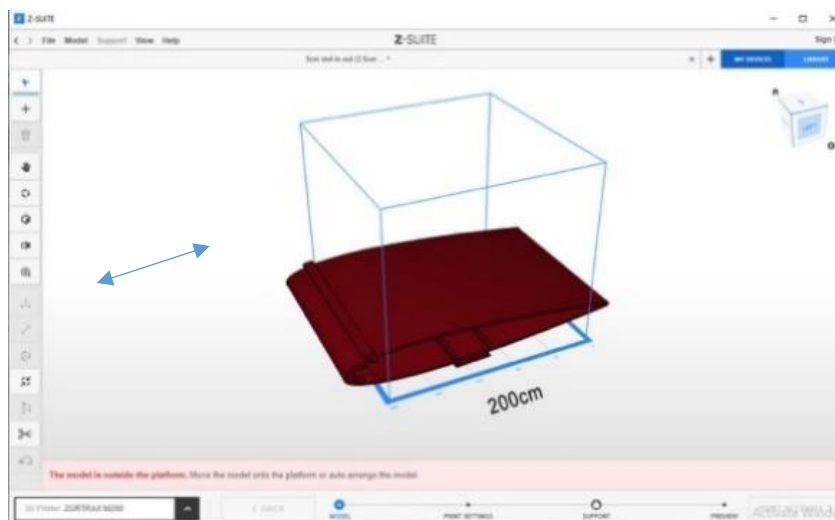


Figure 6 NACA 0012 drawing with chord of 200cm

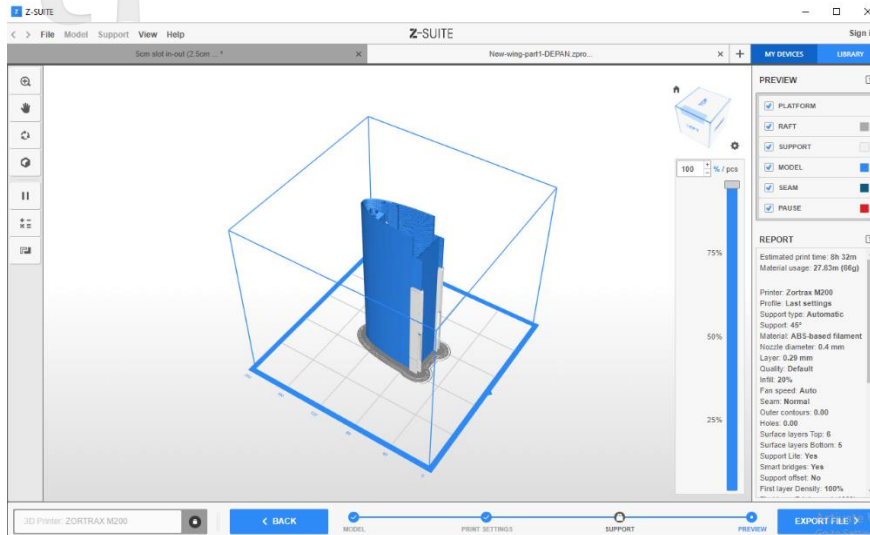


Figure 7 Leading edge part for 3D printing

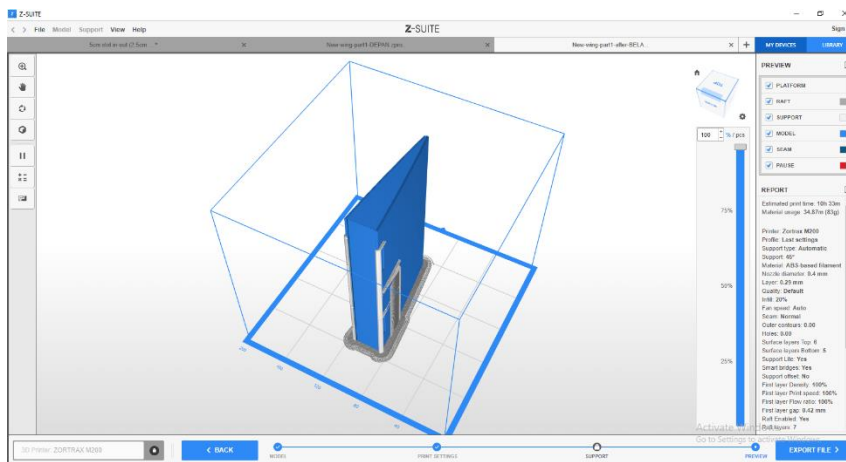


Figure 8 Trailing edge part for 3D printing

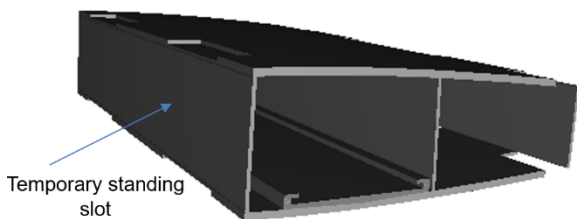


Figure 9 3D drawing for middle part of the wing model

For the manufacturing of the wing, a removable slot for the attachment of the SMA wire inside the airfoil was added to the design. The reason behind the slot in-out for the SMA placement was for ease of assembly. This was also to ease the maintenance process if only 1 wire requires replacement, the slot can be taken out and the SMA will then be replaced. With this design, the complexity of the mechanical design was reduced.

3.2 Testing of Shape Memory Alloy Actuator

Flexinol nitinol wire was selected as an actuator for this study. Selection length of SMA depends on the size of the wing. From this case, NACA 0012 with geometry of 170cm x 200cm needs to use 12cm length of SMA. The SMA specifications are shown in Table 2.

For the 1 wire SMA characterization, the voltage power supply was increased up to 4.5V as in Table 3 with increment of 0.5V. Meanwhile, for 6 wires SMA characterization, the voltage supply was increased up to 7V.

Table 3 Voltage power supply increment for 1 wire SMA characterization

Voltage (V)	Current (A)
0	0
0.5	0.01
1.0	0.25

1.5	0.37
2.0	0.52
2.5	0.65
3.0	0.80
3.5	0.92
4.0	1.07
4.5	1.20

For each increment, data of voltage across power resistor, voltage drop across SMA, temperature SMA and strain was taken. Strain gauge was attached to the plate to obtain the strain measurement on the surface of the plate during actuation and the thermocouple was used for the temperature measurement of the SMA wire. All the data was measured using LabVIEW software and NI-DAQ. The input modules used were NI-DAQ 9237 for strain measurement, NI-DAQ 9201 for voltage measurement and NI-DAQ 9211 for temperature measurement.

Table 2 Flexinol® Actuator Wire Technical and Design Data

Diameter Size (mm)	Resistance (ohms/meter)	Heating Pull Force* (grams)	Cooling Time 158°F, 70°C "LT" Wire*** (seconds)	Cooling Time 194°F, 90°C "HT" Wire*** (seconds)	Austenite Temperature (°C)
0.31	12.2	1280	8.1	6.8	70

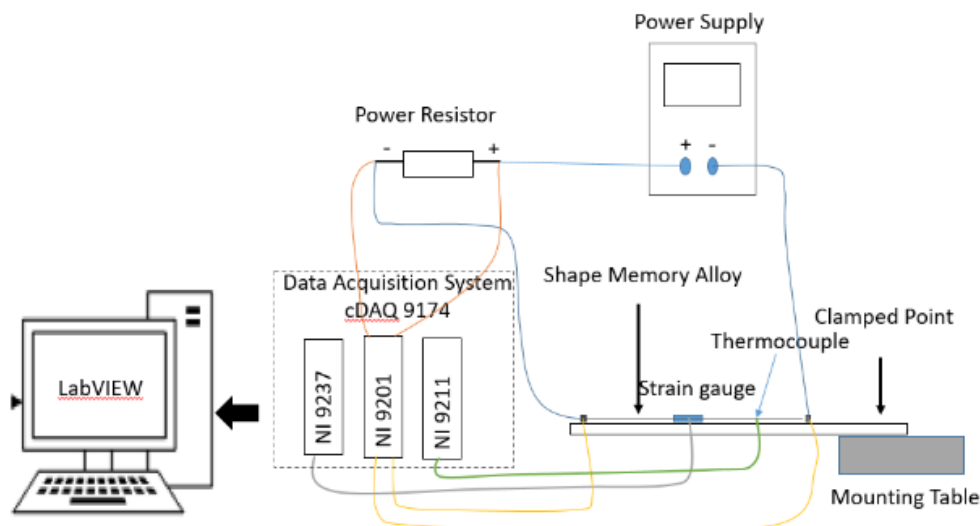


Figure 10 SMA characterization circuit

To measure the current flow across SMA, power resistor was used. With 1 ohm resistance of power resistor in series circuit, the voltage across will be equal to the current across SMA and to other components. If V is the voltage, I is the current and R is the resistance, then

$$\begin{aligned}
 V &= IR \\
 V &= I(1\Omega) \\
 V &= I \\
 V &= \text{Current across SMA}
 \end{aligned}
 \tag{1}$$

Before SMA was embedded inside the wing, SMA characterization is an important aspect to evaluate the voltage drop across SMA for specific displacement. SMA characterization was evaluated on voltage, current, resistance, temperature and strain deflection. 1 wire of 12

cm was tested and the circuit is as shown in Figure 10.

3.3 Wind Tunnel Testing

The test section of the Universiti Putra Malaysia wind tunnel 1m x 1m x 2.5m and the maximum size of the wing is 17cm and 20cm chord and span respectively. The standing slot was designed to mount the wing inside the wind tunnel on the six component balance. Figure 11 shows how the wing was fixed inside the wind tunnel. In Figure 12, it shows the circuit of all the electrical components including the 6 wires SMA embedded in the wing connected with LabVIEW and NI-DAQ. Figure 13 shows the image of 6 wires SMA placed at force node of 3 (upper part) and 37 (lower part). The wing model was installed in the test section of wind tunnel as shown in Figure 14. The calibration angle must be made to ensure

the wing at the exact angle of attack.

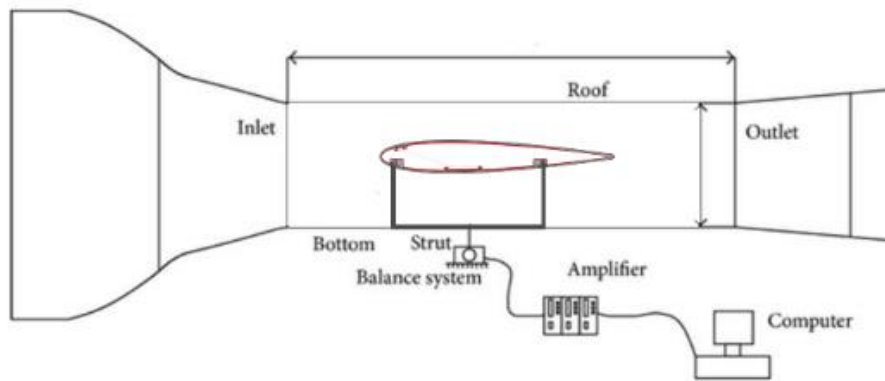


Figure 11 Six-component balance for wind tunnel testing

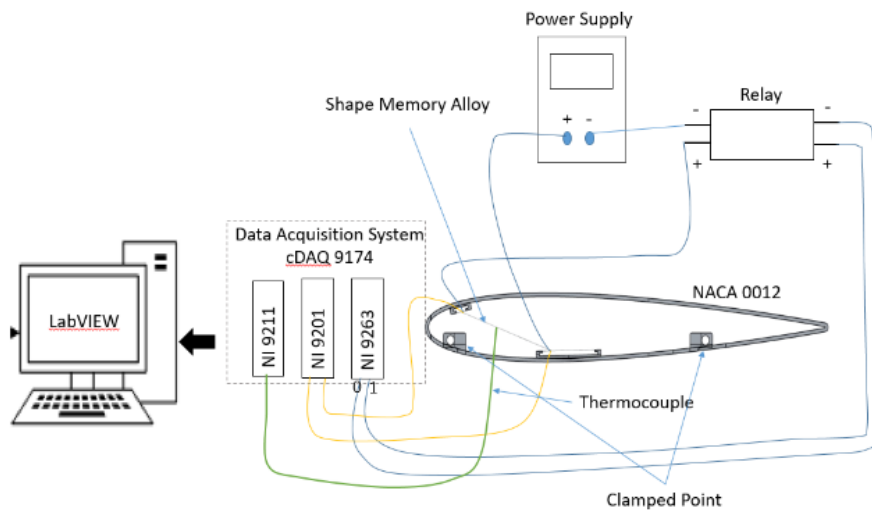


Figure 12 Self-sensing circuit for morphing wing

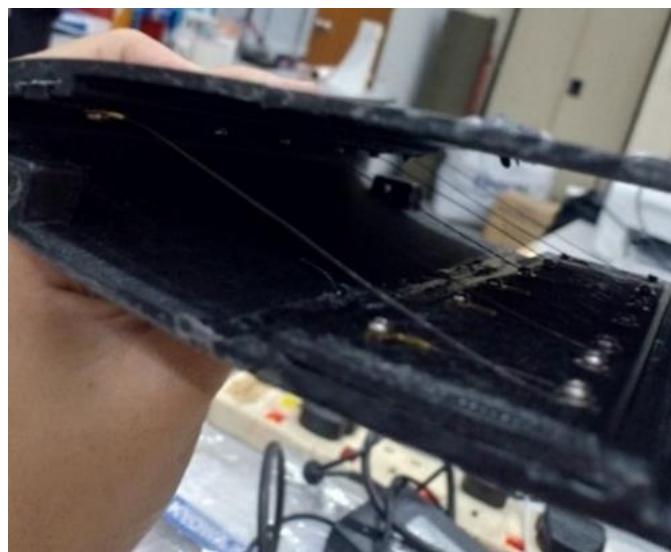


Figure 13 6 wires SMA inside the NACA 0012 wing model

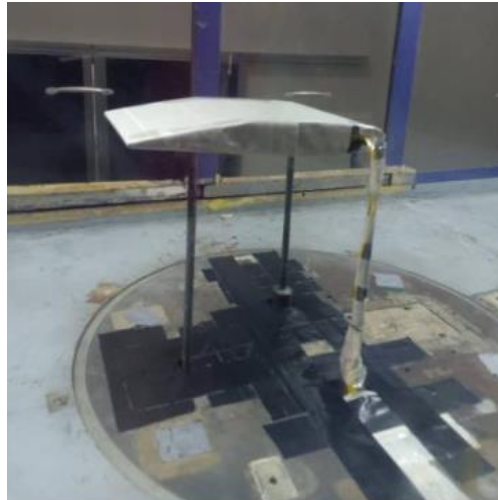


Figure 14 NACA 0012 wing model was installed in the test section

IV. RESULTS AND DISCUSSION

4.1 SMA Characterization

The purpose of SMA characterization is to establish the change in SMA and system's behaviour. For the SMA characterization, it was divided into two parts: 1 wire characterization and 6 wires characterization. 1 wire characterization analysis was to establish the specific characteristics of the wire during heating and cooling as reference for the experimental wing model. 6 wires were the total wires being used inside the morphing wing to achieve the required deflection.

1 SMA wire characterization provided the relationship between the current supplied, temperature of the SMA wire, voltage drop across the SMA wire i.e. change in resistivity and the change in strain or deflection of the wing structure. It is critical to establish this relationship to design the system of the actual wing model. Since the system employs resistance feedback control, it is essential to correlate the voltage drop across the SMA with

the amount of power supplied. Additionally, SMA characterization also will act as a guideline in developing the self-sensing morphing wing for the wind tunnel testing. The characterization data is as shown in Tables 3 and 4.

From Table 4, it shows that during the heating process, the strain was highest at 0.00419 at which temperature reached 48°C where the voltage across SMA was 0.933V. Since the power resistor was arranged in series with the SMA wire, the current of SMA was equal to the current across power resistor. The resistance of the power resistor was 1 ohm, thus the current can be calculated to be 0.844A as the voltage was 0.844V. Resistivity of the SMA can then be calculated to be 1.105Ω. For this set of data, the value of power supply was 3V at 0.8A which was much higher than the voltage across SMA. This was due to the series connection of SMA wire with other components in the circuit such as Ni-DAQ, power resistor and wire. During cooling process, the change in strain was not the same as heating process as expected due to hysteresis as shown in Table 5. The changes of strain decreased gradually as the power supply was decreased.

Table 4 SMA characterization for 1 wire during heating

Volt Power supply	Current (A), Power supply	Voltage drop across Power Resistor (V)	Voltage drop across SMA (V)	Temperature SMA (°C)	Strain
0	0	0.029	0.070	32	0
0.5	0.01	0.120	0.186	32	0
1.0	0.25	0.259	0.321	34	0.00013
1.5	0.37	0.387	0.501	36	0.00033
2.0	0.52	0.536	0.696	40	0.00029
2.5	0.65	0.68	0.845	43	0.00219
3.0	0.80	0.844	0.933	48	0.00419
3.5	0.92	0.973	1.000	52	0.00419
4.0	1.07	1.120	1.200	60	0.00419
4.5	1.20	1.270	1.370	68	0.00409

Table 5 SMA characterization for 1 wire during cooling

Volt Power supply	Current (A), Power supply	Voltage drop across Power Resistor (V)	Voltage drop across SMA (V)	Temperature SMA (°C)	Strain
0	0	0.07	0.03	32	0.00199
0.5	0.12	0.12	0.162	32	0.00228
1	0.27	0.284	0.352	34	0.00285
1.5	0.39	0.48	0.506	36	0.00331
2	0.52	0.526	0.619	38	0.00348
2.5	0.65	0.685	0.768	42	0.00363
3	0.8	0.844	0.912	48	0.00376
3.5	0.92	0.988	1.05	52	0.003848
4	1.07	1.08	1.23	62	0.00399
4.5	1.2	1.27	1.37	68	0.00409

The change of strain on the plate with increment of voltage across the SMA is shown in Figure 15. It can be seen that during the heating process the plate actuated rapidly after Vd reached 0.696V and current of 0.536A at the temperature 40°C. From the result, it can be seen that at least 0.845V and 0.68A was required to change the SMA

NiTi wire phase to austenite which shortened the length of SMA. It also started to maintain its highest peak of 0.00419 strain throughout the process even though Vd kept on increasing. Thus, the Vd value of 0.933V at 0.844A was enough to actuate the SMA and plate to achieve the maximum deflection.

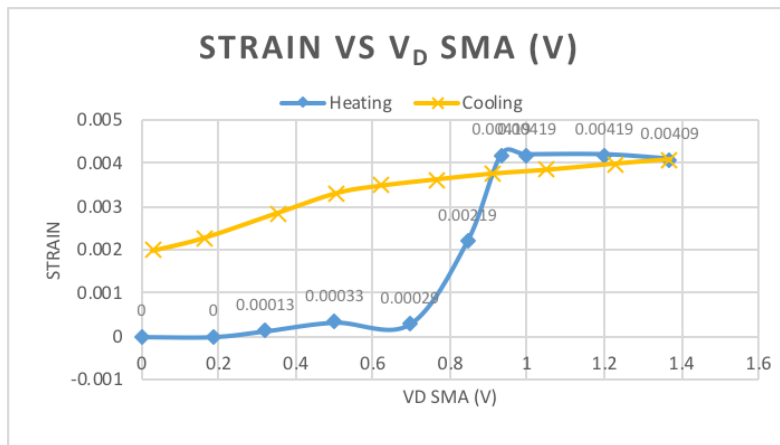


Figure 15 Strain against Voltage drop across 1 SMA wire

Table 6 SMA characterization for 6 wire during heating

Voltage Power supply (V)	Current Power supply (A)	Voltage Power Resistor (V)	Voltage across SMA (V)	Temperature SMA (°C)
0.00	0.00	0.003	0.002	26.90
0.50	0.04	0.053	0.480	27.50
1.00	0.07	0.084	0.809	27.30
1.50	0.12	0.084	0.809	27.30
2.00	0.17	0.207	1.616	29.10
2.50	0.21	0.258	1.920	31.50
3.00	0.26	0.315	2.340	33.90
3.50	0.30	0.361	2.690	36.00
4.00	0.33	0.418	3.080	38.00
4.50	0.37	0.500	3.510	40.69
5.00	0.42	0.562	3.850	41.57
5.50	0.46	0.562	4.300	47.84
6.00	0.57	0.633	4.500	54.93
6.50	0.64	0.690	4.810	66.00
7.00	0.67	0.721	5.380	66.00

Table 7 SMA characterization for 6 wire during cooling

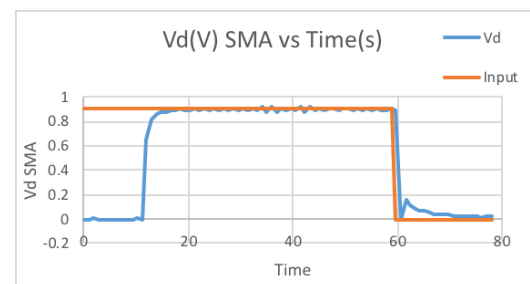
Voltage Power supply (V)	Current Power supply (A)	Voltage Power Resistor (V)	Voltage across SMA (V)	Temperature SMA (°C)
0.00	0.00	0.002	0.002	27.35
0.50	0.04	0.048	0.347	27.90
1.00	0.07	0.150	1.140	29.22
1.50	0.12	0.150	1.140	29.20
2.00	0.17	0.186	1.540	31.00
2.50	0.21	0.222	1.870	32.60
3.00	0.26	0.279	2.250	34.00
3.50	0.30	0.346	2.590	37.00
4.00	0.33	0.397	3.000	40.47
4.50	0.37	0.440	3.500	45.69
5.00	0.42	0.500	3.810	46.00
5.50	0.46	0.536	4.170	47.00
6.00	0.57	0.618	4.520	53.00
6.50	0.64	0.644	5.000	57.00
7.00	0.67	0.711	5.320	65.00

The characterization data as in Tables 6 and 7 can be used to design the morphing wing system using suitable voltage drop for the step input to be used for the wind tunnel testing. The best step input was compared with data 1 wire characterization in Table 4. From Table 4, the best step input selected is at lowest strain value where it began to deflect at 0.00029 strain and 40°C and highest deflection at 0.000409 strain and 68°C. From this comparison, the best step input for 6 SMA wires selected is according to temperature for 1 SMA wire. Step input $V_d = 3.5V$ and $V_d = 4.8V$ were selected to correlate with the 1 SMA wire characterization.

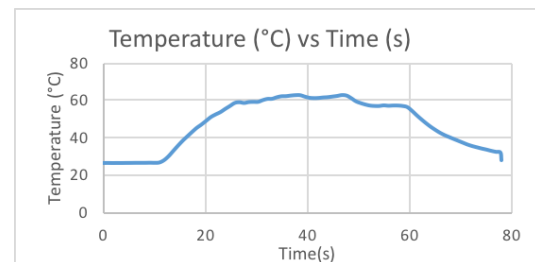
4.2 Feedback Control Results

The results from SMA characterization was analyzed and implemented in the feedback with PID control system to distinguish determine the best PID gain. Different PID controller characteristics was analyzed based on step input of 0.6V, 0.7V, 0.8V and 0.9V. The delay time, T_d , rise time, T_r , overshoot, %OS, peak time, T_p , and settling time, T_s , of voltage feedback controller could be determined. The project objective was to design the PID controller with the smallest error, fast response time and low overshoot. Each test was divided into 2 phases: the wire was heated by the current to achieve the desired step input (3.5V and 4.8V), for the first 60 seconds followed by 20 seconds of applying 0V step input so that the wire is allowed to cool completely prior to the next run.

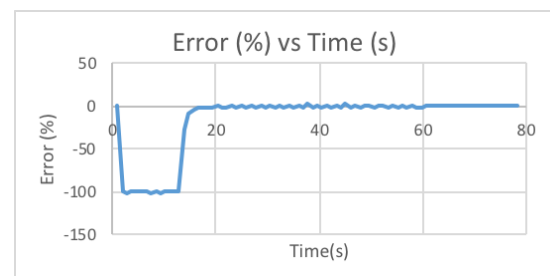
Figure 16 shows the result of voltage drop, temperature and error from the second set of controller using $K_c = 1.2$, $T_i = 0.010$, $T_d = 0.000$ at step input 0.9.



(a)



(b)

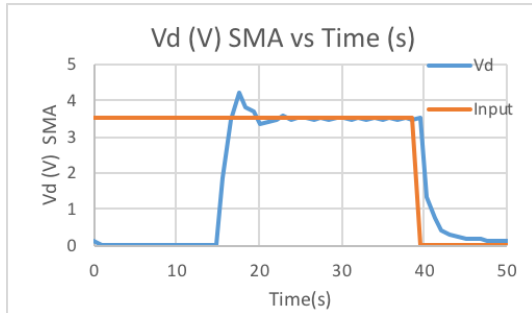


(c)

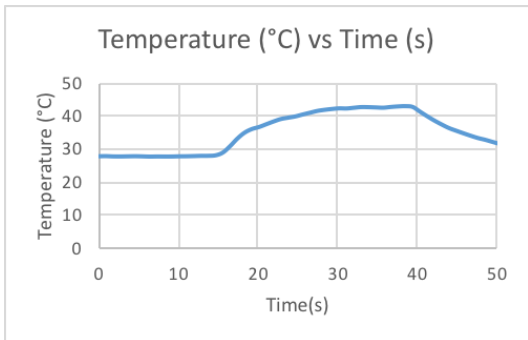
Figure 16 PID step response for (a) Voltage drop across SMA, (b) Temperature, (c) Error at 0.9V with $K_c = 1.200$

Figure 17 shows the result of voltage drop, temperature and error from the second set of controller using $K_c=0.075$ $T_i=0.003$ $T_d=0.02$ at step input 3.5V.

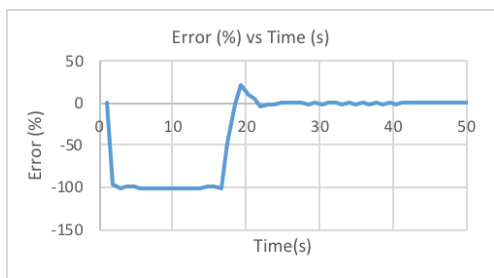
For the first PID with gain $K_c = 1.0$ as shown in Table 8, all the step input had low overshoot percentage of not more than 5%. But the delay time was high compared to other PID. Peak time and delay time were the highest when step input was 0.7V. This step input produced high percentage of overshoot of 3.9%. This system is considered stable as the error was low but in terms of response time, it was very high thus not favourable for the actuation system that required fast response time.



(a)



(b)



(c)

Figure 17 PID step response for (a) Voltage drop across SMA, (b) Temperature, (c) Error at 3.5V with $K_c=0.075$

From the results, PID with gain $K_c = 1.2$ had the best performance compared to 1.0 and 1.5. The response was fast with lowest delay time as step input goes higher, lowest rise time, and lowest settling time. Settling time for 0.9V was 14.78s while $K_c = 1.0$ required 23s compared to $K_c = 1.0$ at 17s. But in terms of overshoot, this PID had high error ranging from 2.5%-9%. As step input increased,

the error reduced. This also shows in $K_c = 1.0$ where the overshoot error reduced when higher step input was used.

For PID $K_c = 1.5$, the control system performance was deemed unacceptable. The delay time and rise time was short which indicated that is good for actuation but the steady state error was as high as 23% and fluctuated. From the presented data, it was demonstrated that higher K_i can decrease the response time but it may increase steady state error.

Table 8 Performance of self-sensing control system for 1 SMA wire for different step input

PID	V _d (V)	Delay time (s)	Rise time (s)	Over-shoot value (V)	Over-shoot (%)	Peak time (s)	Settling time (s)
$K_c=1.0$ $T_i=0.010$ $T_d=0.000$	0.6	21.75	22.67	0.019451	3.24	52.37	24.45
	0.7	18.17	19.98	0.027335	3.90	21.79	22.68
	0.8	15.48	17.26	0.030081	3.76	20.01	23.5
	0.9	17.38	18.31	0.022553	2.51	57.67	23.76
$K_c=1.2$ $T_i=0.010$ $T_d=0.000$	0.6	18.27	19.17	0.04039	6.67	43.68	20.08
	0.7	15.57	15	0.063296	9.04	17.37	20.99
	0.8	12.87	14.7	0.035218	4.40	37.68	39.47
	0.9	12.00	12.92	0.022553	2.51	35.95	14.78
$K_c=1.5$ $T_i=0.010$ $T_d=0.000$	0.6	14.46	14	0.086236	14.37	16.26	27.94
	0.7	11.79	12	0.047884	6.84	14.50	Unsteady
	0.8	11.03	10.5	0.096866	20.46	51.22	Unsteady
	0.9	9.24	11	0.21263	23.62	11.97	Unsteady

Table 9 Performance of self-sensing control system for 6 SMA wires for different step input

PID	V _d (V)	Delay time (s)	Rise time (s)	Overhoot value (V)	Peak time (s)	Settling time (s)
$K_c = 0.075$ $T_i = 0.002$ $T_d = 0.015$	3.5	10.0228	10.5	5.15 (47%)	10.9	14.5855
	4.8	7.35953	8.26296	5.412563 (12.5%)	10.0453	12.8040
$K_c = 0.070$ $T_i = 0.003$ $T_d = 0.02$	3.5	15.6414	16.5387	4.225844 (20.57%)	17.4565	21.1008
	4.8	10.9388	12	5.294405 (10.20%)	14.6212	16.4434

4.3 Wind Tunnel Results

The wind tunnel tests were conducted at low speed wind tunnel with flow velocity of 20m/s. The ambient test condition temperature was 30°C, atmospheric pressure of 101.1kPa and air density of 1.255kg/m³. The angle of attack was varied from at -12° to 16° with increment of 2°. For each test, the data was taken at 0V (not actuated), and step input of 3.5V and 4.8V. The data was collected from DARCS software where the drag coefficient, C_D and lift coefficient, C_L values were calculated based on force axis in x-direction, F_x and z-direction, F_z . The graph of C_L was compared against the angle of attack at 20m/s of airspeed as shown in Figure 20 for three conditions; without actuation, actuated at 3.5V and actuated at 4.8V.

As shown in Figure 18, from angle -12° to -2°, C_L did not show any differences or improvements between actuated and non-actuated condition. The improvement of C_L was at zero degrees angle of attack with increment of 0.010. At 2°, 4°, 6°, C_L increment of 0.037, 0.038 and 0.065 respectively were observed. Table 10 shows the the

changes in C_L for the wing when it was actuated at 4.8V

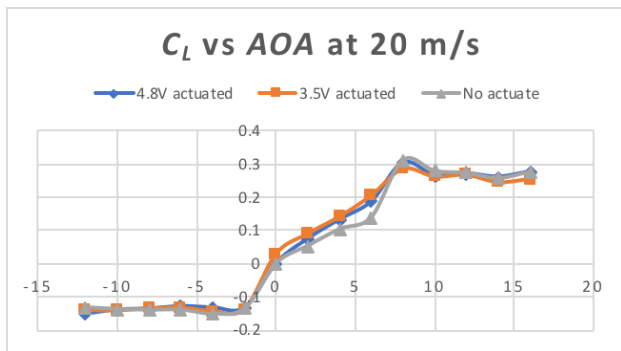


Figure 18 Graph C_L against angle of attack at 20m/s from experimental results

Table 10 Changes in lift coefficient at 4.8V due to SMA actuation

Angle of attack	Lift Coefficient 0V	C_L 4.8V	ΔC_L	% increase
0	0.019	0.029	0.010	51.34836035
2	0.053	0.090	0.037	69.98866767
4	0.103	0.142	0.038	36.91355499
6	0.140	0.205	0.065	46.75214085
8	0.312	0.285	-0.027	-8.562154076

Figure 19 shows the change in C_D for the wing without and with actuation at 3.5V and 4.8V. It can be observed that drag coefficient reduced for all angle of attack for 3.5V and 4.8V step input. This shows great improvement as drag was reduced for all angles of attack when SMA was actuated.

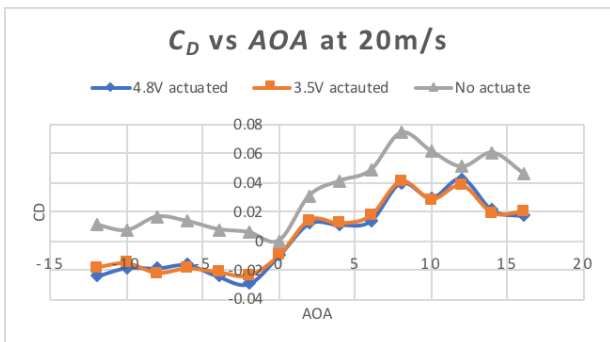


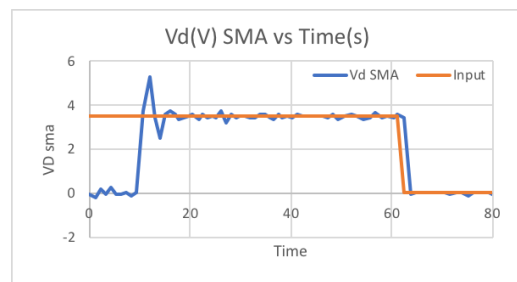
Figure 19 Graph C_D against angle of attack at 20m/s from experimental results

In Table 11, the results show that the actuated morphing wing improves the aerodynamic performance with angle of attack compared with the non-actuated. L/D ratio at cruise angle of 2° improves at 4.55 while 4.8V at 4.39. At angle 4° and 6° also shows improvement as much as 9 and 10 L/D. While at 8° , the L/D decreased, and this may be due to stall at 8° as shown in drag coefficient graph in Figure 19. Thus, we can say this data proves the concept that morphing wing with SMA actuator can improve the aerodynamic performance at different angle of attack.

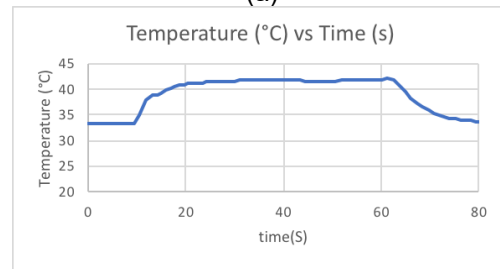
Table 11 Changes in lift-to-drag ratio

AOA ($^\circ$)	L/D 0V	L/D 3.5V	L/D 4.8V	$\Delta L/D$ 3.5V	$\Delta L/D$ 4.8V
0	0.97375	-2.94712	-0.00027	-3.92087	-0.97402
2	1.710559	6.268822	6.103591	4.558263	4.393032
4	2.515051	11.7299	11.7144	9.214849	9.199351
6	2.882561	11.88592	13.67657	9.003364	10.79401
8	4.199324	6.968785	7.622421	2.769461	3.423097

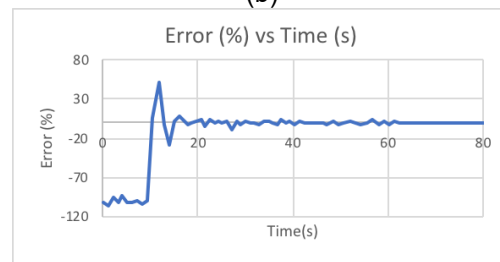
Figures 20 and 21 show the performance of the self-sensing system during wind tunnel testing. Then further analysis on PID performance to compare with the performance with no wind loading. This is vital to compare the efficiency of the system under wind loading.



(a)

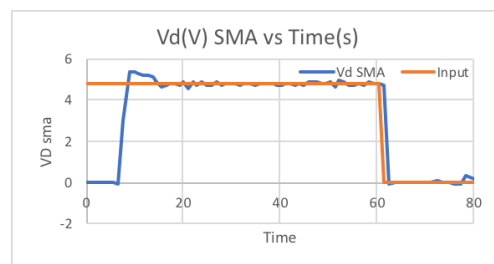


(b)



(c)

Figure 20 3.5V step response under wind loading for; (a) Voltage drop across SMA, (b) Temperature, (c) Error for $K_c=0.075$, $T_i= 0.002$ $T_d= 0.015$



(a)

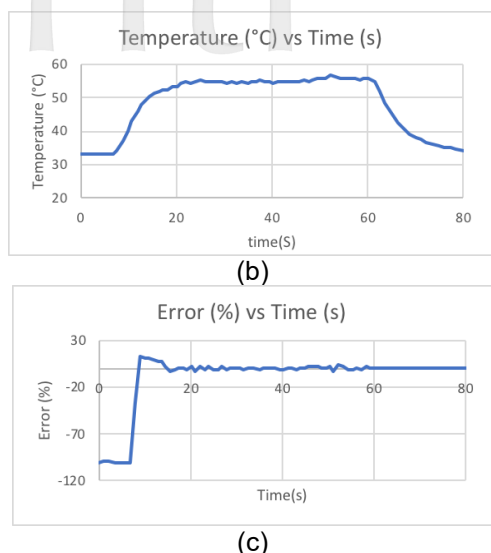


Figure 21 3.5V step response under wind loading for; (a) Voltage drop across SMA, (b) Temperature, (c) Error for $K_c=0.075$

From Table 12, it can be seen that 4.8V step input has shorter delay, rise time, peak time and settling time compared with 3.5V step input. Both step inputs also have overshoot exceeding 5V which are 5.32V and 5.4V respectively. This PID characteristics behavior shows the same pattern as in Table 8 with difference of only around 1-2s for all the characteristics. The step response of the self-sensing morphing wing without or with wind loading shows that the higher the step input, the shorter the delay, rise, peak and settling time. The controller developed performed effectively in the wind tunnel tests even in the presence of wind loading.

Table 12 Experimental test performance of self-sensing morphing wing for different step input

PID	V_d (V)	Delay time (s)	Rise time (s)	Overshoot value (V), (Error %)	Peak time (s)	Settling time (s)
$K_c = 0.0075$ $T_i = 0.002$ $T_d = 0.015$	3.50	9.37	10.50	5.32, (52%)	11.89	15.00
	4.80	6.70	8.00	5.40, (12%)	8.85	14.50

From the wind tunnel testing, the data shows the difference of drag and lift coefficient without and with actuation. This proves that the self-sensing system's performance was acceptable under wind loading with speed of 20m/s. Improvements of drag and lift was recorded when the wing morphed at certain angle before it stalls. The highest improvement of L/D was at angle of attack of 6° with values of 10.79 for 4.8V step input before it stalls at 8° . For un-morphed condition, it produced the highest L/D at 8° and stalled at 12° . For the PID controller, the actuation performance was the best with the presence of wind loading. The error recorded was less than 2% during the settling time.

V. CONCLUSIONS

A self-sensing morphing wing system using shape memory alloy has been developed in the research presented here. The development involves multidisciplinary design involving aerodynamics, material, structure, design, fabrication, control and system integration. The test bed for morphing wing was limited due to the size of the test section of the wind tunnel. The minimum size was set to 17cm x 200cm and produced into 3 parts for ease of fabrication due to 3D printer limitation. The design and fabrication of the morphing wing system was critical to ensure easy integration of SMA inside the wing.

The change of resistivity during actuation was successfully utilized as the input to the feedback system with a PID controller. The performance of the system was excellent with low delay, rise, peak and settling time. Even though overshoot was high, the temperature was the same indicating that phase changes of SMA did not occur. Thus, it is feasible to use shape memory alloy as both sensor and actuator for the morphing wing system without any additional sensor, thus reducing the weight and cost of the system.

The wing model was tested at angle of attack between -12° and 16° at wind speed of 20m/s. The experimental results of wind tunnel testing showed that the morphing wing system produced improvement on lift, drag and lift-to-drag ratio as predicted from earlier work using computational fluid dynamics. L/D improved as much as 9.2 at 4° AOA for SMA actuation of 3.5V and 10.79 at 6° AOA for SMA actuation of 4.8V. PID controller built for SMA characterization can be used for wind tunnel testing as shown in the results. The performance of the controller was excellent even under the presence of wind loading.

Further improvements on the system developed in this research can be achieved by analysing larger range of actuation, using larger wing span for increased accuracy of aerodynamics data, improving the fabrication technique, manufacturing and integration of SMA wire for a larger ease of maintenance and comparing the performance of the self-sensing system with strain feedback and temperature feedback in order to design the optimal morphing wing system using shape memory alloy actuator.

ACKNOWLEDGMENTS

The authors would like to acknowledge that the research findings presented in this paper was funded by Research University Grant Scheme (RUGS) UPM/700-2/1/GPB/2017/9530800 from Universiti Putra Malaysia.

REFERENCES

- [1] Balakrishnan S, Basri AA, Basri EI, Yazik MHBM. "Effects of Different Thickness of UAV Airfoil on Aerodynamics Performance Using CFD Techniques," *Journal of Aeronautics, Astronautics and Aviation*, Vol. 53, No. 2, 2021, pp. 275-282. [https://doi.org/10.6125/JoAAA.202106_53\(2\).20](https://doi.org/10.6125/JoAAA.202106_53(2).20)

- [2] Zaini H, Ismail NI, "A Review of Morphing Wing," International Conference in Mechanical Engineering Colloquium, School of Mechanical Engineering, University of Liverpool, Liverpool, England, August, 2016. Accessed Jan. 20, 2025. [Online]. Available: https://www.researchgate.net/profile/Noor-Iswardi-Ismail/publication/308647301_A_Review_of_Morphing_Wing/links/57ea0e3508aef8bfcc96334c/A-Review-of-Morphing-Wing.pdf
- [3] Urnes J, Ippolito C, Totah J, Ting E, "A Mission-Adaptive Variable Camber Flap Control System to Optimize High Lift and Cruise Lift-to-Drag Ratios of Future N + 3 Transport Aircraft," 51st AIAA Aerospace Sciences Meeting including the New Horizons Forum and Aerospace Exposition, January 2013. <https://doi.org/10.2514/6.2013-214>
- [4] Hussain SA, "Review of Morphing Wing," B.Eng in Aerospace Engineering Thesis, Coventry University, May 2017. Accessed Jan. 20, 2025. [Online]. Available: https://www.researchgate.net/publication/328655295_Review_of_Morphing_Wing
- [5] Barbarino SI, Bilgen O, Ajaj RM, Friswell M, Inman D, "A Review of Morphing Aircraft," *Journal of Intelligent Material Systems and Structures*, Vol. 22, No. 9, 2011, pp. 823-877. <https://doi.org/10.1177/1045389X11414084>
- [6] Prisacariu V, Boşoianu M, Cîrciu I, "Morphing Wing Concept for Small UAV," *Applied Mechanics and Material*, Vol. 332, 2013, pp. 44-49. <https://doi.org/10.4028/www.scientific.net/AMM.332.44>
- [7] Bil C, Massey K, and Abdullah EJ, "Wing morphing control with shape memory alloy actuators," *Journal of Intelligent Material Systems and Structures*, Vol. 24, No. 7, 2013, pp. 879-898. <https://doi.org/10.1177/1045389X12471866>
- [8] Imran HY, Majid DLAA, Hamid MFA, Abdullah EJ, Mohammed SE, Karunakaran S, "Thermomechanical Performance of Shape Memory Alloy Spring by Homogeneous Distribution of Temperature," *Journal of Aeronautics, Astronautics and Aviation*, Vol. 56, No. 1S, 2024, pp. 117-124. [https://doi.org/10.6125/JoAAA.202403_56\(1S\).04](https://doi.org/10.6125/JoAAA.202403_56(1S).04)
- [9] Karunakaran S, Majid, DLAA, Imran HY, "Superelasticity Behaviour of NiTi Actuator at Different Strain Rates," *Journal of Aeronautics, Astronautics and Aviation*, Vol. 56, No. 1S, 2024, pp. 107-115. [https://doi.org/10.6125/JoAAA.202403_56\(1S\).03](https://doi.org/10.6125/JoAAA.202403_56(1S).03)
- [10] Abdullah EJ, Majid DL, Romli FI, Gaikwad PS, Yuan LG, Harun NF, "Active Control of Strain in Composite Plate Using Shape Memory Alloy Actuators," *International Journal of Mechanics and Materials in Design*, Vol. 11, No. 1, 2015, pp. 25-39. <https://doi.org/10.1007/s10999-014-9277-7>
- [11] Abdullah EJ, Gaikwad PS, Azid N, Abdul Majid DL, Mohd Rafie AS, "Temperature and Strain Feedback Control for Shape Memory Alloy Actuated Composite Plate," *Sensors and Actuators A: Physical*, Vol. 283, 2018, pp. 134-140. <https://doi.org/10.1016/j.sna.2018.09.059>
- [12] Amir S, Abdullah EJ, "Multidisciplinary Design of a High Lift Device using Shape Memory Alloy Actuator," *Journal of Aeronautics, Astronautics and Aviation*, Vol. 56(1S), 2024, pp. 257-266. [https://doi.org/10.6125/JoAAA.202403_56\(1S\).1](https://doi.org/10.6125/JoAAA.202403_56(1S).1)
- [13] Ruth DSJ, Dhanalakshmi K, "Shape Memory Alloy Wire for Self-Sensing Servo Actuation," *Mechanical Systems and Signal Processing*, Vol. 83, No. 15, 2017, pp. 36-52. <https://doi.org/10.1016/j.ymsp.2016.05.042>
- [14] Ruth DSJ, Dhanalakshmi K, Nakshatharan SS, "Bidirectional Angular Control of an Integrated Sensor/Actuator Shape Memory Alloy Based System," *Measurement*, Vol. 69, 2015, pp. 210-221. <https://doi.org/10.1016/j.measurement.2015.02.058>
- [15] Narayanan P, Elahinia M, "Control of a Shape Memory Alloy-Actuated Rotary Manipulator using an Artificial Neural Network-Based Self-Sensing Technique," *Journal of Intelligent Material Systems and Structures*, Vol. 27, No. 14, 2016, pp. 1885-1894. <https://doi.org/10.1177/1045389X15596626>
- [16] Gurung H, Banerjee A, "Self-sensing Shape Memory Alloy Wire Actuator Based on Unscented Kalman Filter," *Sensors and Actuators A: Physical*, Vol. 251, 2016, pp. 258-265. <https://doi.org/10.1016/j.sna.2016.09.037>
- [17] Sakagami T, Seki K, Iwasaki M, "Sensorless Position Control Based on Resistance and Heat Transfer Models in Shape Memory Alloy Actuators," *IEEE/ASME International Conference on Advanced Intelligent Mechatronics*, Vol. 2019, July 2019, pp. 217-222. <https://doi.org/10.1109/AIM.2019.8868335>
- [18] Lee SH, Kim SW, "Improved Position Control of Shape Memory Alloy Actuator using the Self-Sensing Model," *Sensors and Actuators, A: Physical*, Vol. 297, 2019, 111529. <https://doi.org/10.1016/j.sna.2019.111529>
- [19] Butt JR, "A Study of Morphing Wing Effectiveness in Fighter Aircraft using Exergy Analysis and Global Optimization Techniques," MSc in Mechanical Engineering Thesis, Virginia Tech, 2005. Accessed Jan., 20, 2025. [Online]. Available: <http://hdl.handle.net/10919/36368>
- [20] Janker P, Claeysen F, Grohmann B, Christmann M, Lorkowski T, LeLetty R, Sosniki O, Pages A, "New Actuators for Aircraft and Space Applications," Proceedings of the 11th International Conference on New Actuators, Bremen, Germany, 2008, pp. 9-11. Accessed Jan., 20, 2025. [Online]. Available: https://www.researchgate.net/publication/242683601_New_Actuators_for_Aircraft_and_Space_Application
- [21] Gilyard GB, "Estimated Benefits of Variable-Geometry Wing Camber Control for Transport Aircraft," NASA technical memorandum, 1999, 206586. Accessed Jan., 20, 2025. [Online]. Available:

- <https://ntrs.nasa.gov/api/citations/19990090019/downloads/19990090019.pdf>
- [22] Azid N, Manan DA, Tet NW, Abdullah EJ, Abdul Majid DL, "Design Fabrication of Adaptive Wing Structure," *International Journal of Innovative Technology and Exploring Engineering*, Vol. 9, No. 3, 2020, pp. 2656-2659.
<https://doi.org/10.35940/ijitee.C8802.019320>
- [23] Leahy M, "Multidisciplinary Design Optimization of a Morphing Wingtip Concept with Multiple Morphing Stages at Cruise," MSc Thesis, University of Toronto, 2013. Accessed Jan., 20, 2025. [Online]. Available:
<http://hdl.handle.net/1807/43002>
- [24] Sinn T, Barrett R, "Design, Manufacturing and Test of a High Lift Secondary Flight Control Surface with Shape Memory Alloy Post-Buckled Precompressed Actuators," *Actuators*, Vol. 4 No. 3, 2015, pp. 156-171.
<https://doi.org/10.3390/act4030156>
- [25] Lee SY, Lee GY, "Largely Deformable Torsional Soft Morphing Actuator Created by Twisted Shape Memory Alloy Wire and its Application to a Soft Morphing Wing," *Scientific Reports*, Vol. 13, 2023, 17629.
<https://doi.org/10.1038/s41598-023-44936-4>
- [26] Ozbek E, Ekici S, Karakoc TH, "Unleashing the Potential of Morphing Wings: A Novel Cost Effective Morphing Method for UAV Surfaces, Rear Spar Articulated Wing Camber," *Drones*, Vol. 7, No. 6, 2023, 379.
<https://doi.org/10.3390/drones7060379>
- [27] Grigorie TL, Botez RM, "A Self-Tuning Intelligent Controller for a Smart Actuation Mechanism of a Morphing Wing Based on Shape Memory Alloys," *Actuators*, Vol. 12, No. 9, 2023, 350.
<https://doi.org/10.3390/act12090350>
- [28] Manan DA, "Design and Fabrication of Hybrid Composite Adaptive Wing Structure," B.Eng. Degree Thesis, Universiti Putra Malaysia, 2008.
- [29] Liu Y, "On the Detwinning Mechanism in Shape Memory Alloys," IUTAM Symposium on Mechanics of Martensitic Phase Transformation in Solids. Solid Mechanics and Its Applications, Vol. 101, 2002.
https://doi.org/10.1007/978-94-017-0069-6_5
- [30] Botez RM, "Morphing Wing , UAV and Aircraft Multidisciplinary Studies at the Laboratory of Applied Research in Active Controls , Avionics and AeroServoElasticity LARCASE," *AerospaceLab Journal*, ONERA, 2018, pp. 1-11. Accessed Jan., 20, 2025. [Online]. Available:
<https://aerospacelab.onera.fr/en/al14/morphing-wing-uav-and-aircraft-multidisciplinary-studies>
- [31] Pai A, Riepold M, Trachtler A, "A Model Extended Temperature and Strain Controller Modulated with PWM for Precision Position Control of Shape Memory Alloy Actuators," 2016 IEEE International Conference on Advanced Intelligent Mechatronics (AIM), 2016, pp. 442-447.
<https://doi.org/10.1109/AIM.2016.7576807>
- [32] Chouhan P, Nath T, Lad BK, Palani IA, "Investigation on Actuation and Thermo-Mechanical Behaviour of Shape Memory Alloy Spring Using Hot Water," *IOP Conference Series: Materials Science and Engineering*, Vol. 149, 2016, 012147.
<https://doi.org/10.1088/1757-899X/149/1/012147>
- [33] Song H, Kubica E, Gorbet R, "Resistance Modelling of Sma Wire Actuators," *International Workshop Smart Materials Structures & NDT in Aerospace*, 2011. Accessed Jan., 20, 2025. [Online]. Available:
https://www.ndt.net/article/ndtcanada2011/papers/6_6_Gorbet_Rev2.pdf
- [34] Riccardi L, Rizzello G, Naso D, Holz B, Seelecke S, Janocha H, Turchiano B, "Modeling and Control of Innovative Smart Materials and Actuators: A Tutorial," 2014 IEEE Conference on Control Applications (CCA), Juan Les Antibes, France, 2014, pp. 965-977.
<https://doi.org/10.1109/CCA.2014.6981461>
- [35] Wang T, Shi Z, Liu D, Ma C, Zhang Z, "An Accurately Controlled Antagonistic Shape Memory Alloy Actuator with Self-Sensing," *Sensors*, Vol. 12, No. 6, 2012, pp. 7682-7700.
<https://doi.org/10.3390/s120607682>
- [36] Abdullah EJ, Soriano J, Fernández de Bastida Garrido I, Abdul Majid DL, "Accurate Position Control of Shape Memory Alloy Actuation using Displacement Feedback and Self-Sensing System," *Microsystem Technologies*, Vol. 27, 2021, pp. 2553-2566.
<https://doi.org/10.1007/s00542-020-05085-0>